processes

MDPI

*Article*

# Prediction of the Residual Creep Life of SA335-P22 Steel Main Steam Pipelines

**Zhicheng Wang, Youjun Ye *, Lingjian Dong and Bumei Wang**

Special Equipment Safety Supervision and Inspection Institute of Jiangsu Province, Nanjing 210036, China
* Correspondence: ye12youjun@163.com

**Abstract:** In this study, the comprehensive properties of a P22 high-temperature steam pipeline with moderate spheroidization were evaluated after more than 11,700 h of operation through a series of physico-chemical properties testing, especially for a creep test. The remaining life of the P22 high-temperature steam pipeline was analyzed and predicted by the $\theta$ parameter method, to guide the normal operation of the P22 high-temperature steam pipeline.

**Keywords:** P22 high-temperature steam pipeline; remaining life prediction; creep test



**Citation:** Wang, Z.; Ye, Y.; Dong, L.; Wang, B. Prediction of the Residual Creep Life of SA335-P22 Steel Main Steam Pipelines. *Processes* **2023**, *11*, 162. https://doi.org/10.3390/pr11010162

Academic Editors: Antonino Recca and Yoshiei Kato

Received: 23 October 2022
Revised: 22 November 2022
Accepted: 26 December 2022
Published: 4 January 2023



## 1. Introduction

Sa335-P22 steel pipes [1–5] consist of 2.25Cr-1Mo low alloy steel, as this material exhibits good weldability and persistent plasticity, and is mainly used in the pressure bearing system of main-steam pipelines in thermal power plants. A comprehensive inspection of a powerplant (Location: Nanjing, Jiangsu Province) in 2015 found that the metallographic structure of a section of SA335-P22 pipeline was moderately spheroidized. The pipeline was operated at 7800 h per year, and this batch of SA335-P22 pipeline had been in service for about 117,00 h. The dimensions and metallographic examination results of the SA335-P22 material are shown in Table 1. To ensure the safe and continuous operation of SA335-P22 main steam pipelines, the material properties of the SA335-P22 main steam pipeline were comprehensively evaluated through on-site sampling and a series of physical and chemical tests. Compared to the traditional extrapolation prediction method [6–10], the $\theta$ parameter method [11–13] better addresses the entire creep process. Therefore, based on the creep test results, residual creep life evaluation of a SA335-P22 main steam pipeline was conducted by the $\theta$ parameter method.

**Table 1.** The specifications and metallographic examination results of the SA335-P22.

| Material | Medium | Dimension/ Thickness (mm) | Design Temperature (°C) | Design Pressure (MPa) | Working Temperature (°C) | Working Pressure (MPa) | Spheroidization Degree |
|---|---|---|---|---|---|---|---|
| P22 | Steam | 219/20.6 | 524 | 8.5 | 510 | 7.0 | Moderate |

## 2. Physical and Chemical Tests and Result Analysis

The physical and chemical tests consisted of chemical composition analysis [14], mechanical property [15], metallographic analysis [16], hardness, and creep rupture tests [17].

### 2.1. Chemical Composition Analysis

The chemical composition of the SA335-P22 steel pipe was analyzed by energy spectrum analysis. As shown in Table 2, its chemical composition met the ASME SA335 [18] requirements for P22 steel pipes.

**Table 2.** Chemical composition (wt).

| Material | C | Mn | *p* | S | Si | Cr | Mo | Other |
|---|---|---|---|---|---|---|---|---|
| ASME SA335-P22 | 0.05–0.15 | 0.30–0.60 | ≤0.025 | ≤0.025 | ≤0.50 | 1.90–2.60 | 0.87–1.13 | - |
| Result | 0.10 | 0.43 | 0.014 | 0.005 | 0.24 | 2.09 | 0.94 | |
| Conclusion | Meets ASME SA335 requirements for new P22 pipes | | | | | | | |

## *2.2. Mechanical Properties*

### 2.2.1. Tension Test at Room Temperature

The test was carried out according to GB/T 228.1-2010 "Metallic materials tensile test part1 room temperature test method" [19]. The size of the sample is shown in Figure 1, and the test was conducted on a MTS809 tension torsion testing machine. The longitudinal tensile test results are presented in Table 3, and the transverse tensile test results are provided in Table 4. The tensile performance results obtained at room temperature demonstrated that the P22 pipe had poor plastic properties at room temperature, although all indicators met the relevant AEM SA335 requirements.

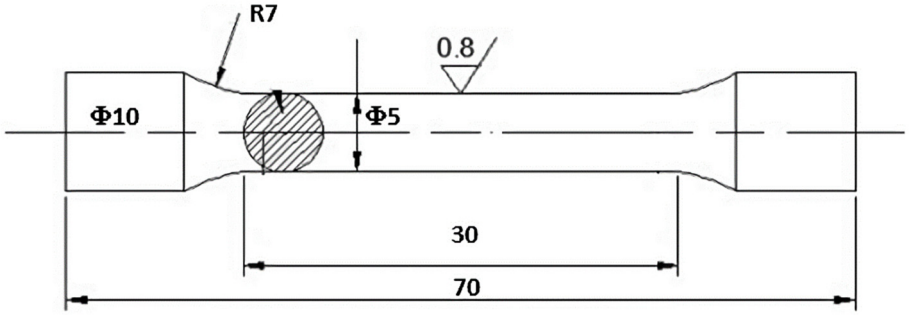


**Figure 1.** The size of the sample at room temperature (mm).

**Table 3.** The results of the longitudinal tensile test.

| Sampling Position | Sample | Rp0.2/MPa | Rm/MPa | A/% |
|---|---|---|---|---|
| SA335/SA335M | - | ≥205 | ≥415 | ≥22 (portrait) |
| Near the outer wall | 1 | 322 | 538 | 31.5 |
| | 2 | 326 | 542 | 28.5 |
| | 3 | 316 | 532 | 26.5 |
| Near the middle wall | 1 | 344 | 553 | 35.0 |
| | 2 | 350 | 559 | 30.5 |
| | 3 | 330 | 534 | 29.5 |
| Near the inner wall | 1 | 334 | 536 | 25.0 |
| | 2 | 349 | 557 | 26.5 |
| | 3 | 351 | 557 | 29.5 |
| Conclusion | Room temperature longitudinal tension meets the requirements of ASME SA335/SA335M for the P22 new pipe | | | |

**Table 4.** The transverse tensile test results.

| Sampling Position | Sample | Rp0.2/MPa | Rm/MPa | A/% |
|---|---|---|---|---|
| SA335/SA335M | - | ≥205 | ≥415 | ≥14 (portrait) |
| Near the middle wall | 1 | 343 | 553 | 25.5 |
| | 2 | 346 | 554 | 28.0 |
| | 3 | 346 | 556 | 28.0 |
| Near the inner wall | 1 | 345 | 544 | 26.0 |
| | 2 | 348 | 546 | 26.0 |
| | 3 | 331 | 541 | 29.0 |

**Table 4.** *Cont.*

| Sampling Position | Sample | Rp0.2/MPa | Rm/MPa | A/% |
|---|---|---|---|---|
| Conclusion | Room temperature longitudinal tension meets the requirements of ASME SA335/SA335M for P22 new pipe | | | |

2.2.2. Tensile Test at High Temperatures

Testing was carried out according to GB/T 228.2-2015 "Metallic materials tensile test part 2 high-temperature test method" [20], and the size of the sample is shown in Figure 2. The test temperatures of the pipe were 540 °C and 580 °C, according to the actual operating conditions and creep test requirements of the pipe. The sample under the high-temperature condition was only selected in the longitudinal direction, and the test was conducted on an MTS809 tension torsion testing machine. Table 5 shows the tensile performance test results at 540 °C, while the tensile performance test results at 580 °C are shown in Table 6.

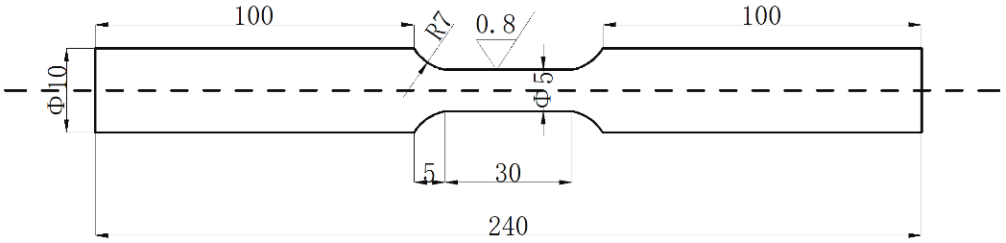


**Figure 2.** The size of the sample at a high temperature (mm).

**Table 5.** The results of the tensile test at 540 °C.

| Sampling Position | Sample | Rp0.2/MPa | Rm/MPa | A/% |
|---|---|---|---|---|
| 12Cr2MoG (500 °C) | - | ≥173 | - | - |
| 12Cr2MoG (550 °C) | - | ≥159 | - | - |
| 10CrMo910 (500 °C) | - | ≥180 | - | - |
| Near the outer wall | 1 | 286 | 442 | 21.5 |
| | 2 | 268 | 427 | 22.5 |
| | 3 | 276 | 432 | 24.0 |
| Near the middle wall | 1 | 301 | 451 | 23.0 |
| | 2 | 278 | 437 | 21.5 |
| | 3 | 286 | 443 | 23.0 |
| Near the inner wall | 1 | 281 | 440 | - |
| | 2 | 301 | 452 | 23.0 |
| | 3 | 305 | 457 | 22.0 |
| Conclusion | The yield strength at 540 °C was higher than 12Cr2M$_O$G at 500 °C in GB/T5310-2017 and 10CrMo910 at 500°C in DL/T999-2006. | | | |

**Table 6.** The tensile test results at 580 °C.

| Sampling Position | Sample | Rp0.2/MPa | Rm/MPa | A/% |
|---|---|---|---|---|
| 12Cr2MoG (500 °C) | - | ≥173 | - | - |
| 12Cr2MoG (550 °C) | - | ≥159 | - | - |
| 10CrMo910 (500 °C) | - | ≥180 | - | - |
| Near the outer wall | 1 | 276 | 431 | 24.0 |
| | 2 | 278 | 424 | 22.5 |
| Near the middle wall | 1 | 281 | 441 | 22.0 |
| | 2 | 275 | 433 | 24.5 |
| | 3 | 279 | 421 | 24.0 |
| Near the inner wall | 1 | 272 | 435 | 23.0 |
| | 2 | 264 | 413 | 25.5 |
| | 3 | 290 | 447 | 20.5 |

**Table 6.** *Cont.*

| Sampling Position | Sample | Rp0.2/MPa | Rm/MPa | A/% |
|---|---|---|---|---|
| Conclusion | The yield strength at 580 °C was higher than 12Cr2M$_O$G at 500 °C in GB/T5310-2017 and 10CrMo910 at 500°C in DL/T999-2006. | | | |

As shown in Tables 5 and 6, the performance of the sample at 540 °C and 580 °C met the requirements for the yield strength of 12Cr2MoG at 500 °C in the seamless steel tubes for high-pressure boilers (GB/T 5310-2017) [21], as well as the requirements for the yield strength of 10CrMo910 at 500 °C in EN10216-2:2002 provided in Appendix C of DL/T 999-2006.

### *2.3. Metallographic Test and Result Analysis*

#### 2.3.1. Metallographic Tests

The sample was 20 mm (length) × original wall thickness (width) × 15 mm (height) in size. The position of the utilized sample is shown in Figure 3, which consisted of four directions perpendicular to each other in the cross-section of the steel pipe (0°, 90, 180, 270°). The sample was prepared by grinding, polishing, and corrosion in accordance with the GB/T 13298-2015 [22] methods for the testing of metal microstructures.

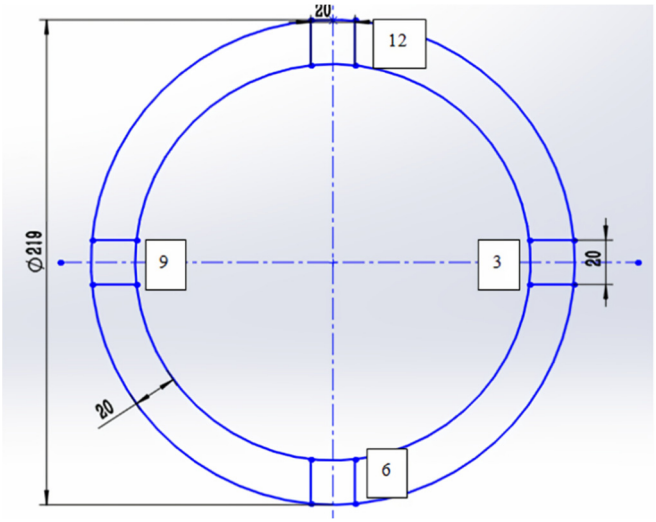


**Figure 3.** Schematic diagram of metallographic sampling position.

#### 2.3.2. Analysis of the Results

According to the previous metallographic tests of the cross-section and longitudinal section, we found no obvious differences in the microstructures of the samples in the four directions (0°, 90, 180, 270°). Therefore, the samples at 0° and 270° were selected for metallographic analysis of the internal and external surfaces.

(1) Metallographic analysis of the external surface

Figures 4 and 5 show the metallographic structure of the outer surface in the 270° and 0°. Through analysis, we could easily determine that the structure was ferrite and bainite. The bainite area had started to disperse, there was no obvious carbide aggregation at the grain boundary, and no creep holes were found in the leaves.

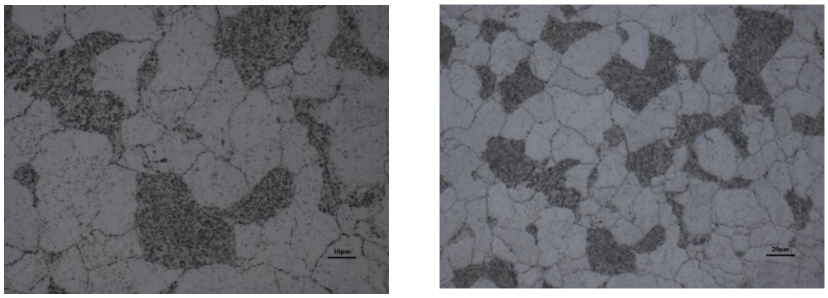

(**a**) (**b**)

**Figure 4.** Metallographic structure of external surface in the 270° direction. (**a**) 500×, (**b**) 1000×.

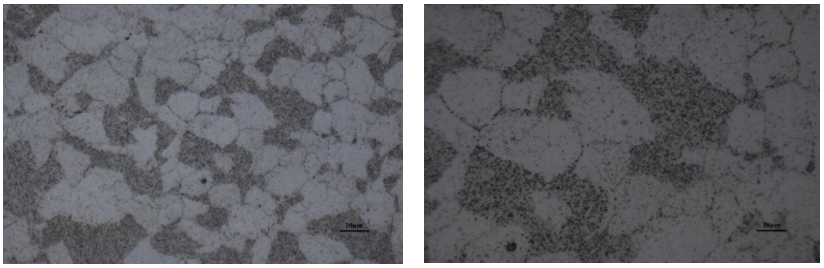

(**a**) (**b**)

**Figure 5.** Metallographic structure of inner surface in the 0° direction. (**a**) 500×, (**b**) 1000×.

(2) Metallographic analysis of the inner surface

Figures 6 and 7 show the metallographic structure of the inner surface in the 270° and 0° directions. Through analysis, we could easily determine that the structure was ferrite and bainite. The bainite area had started to disperse, there was no obvious carbide aggregation at the grain boundary, and there were no creep holes in the leaves.

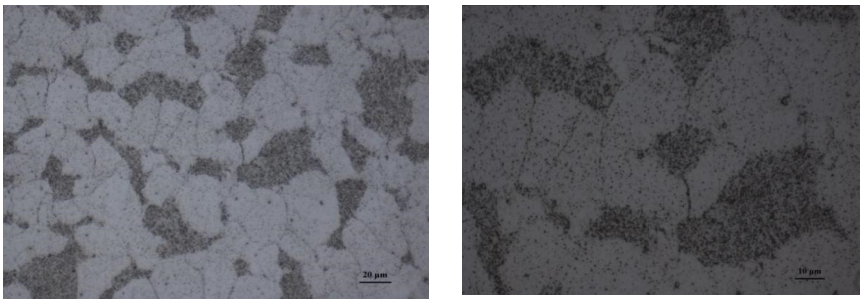

(**a**) (**b**)

**Figure 6.** Metallographic structure of inner surface in the 270° direction. (**a**) 500×, (**b**) 1000×.

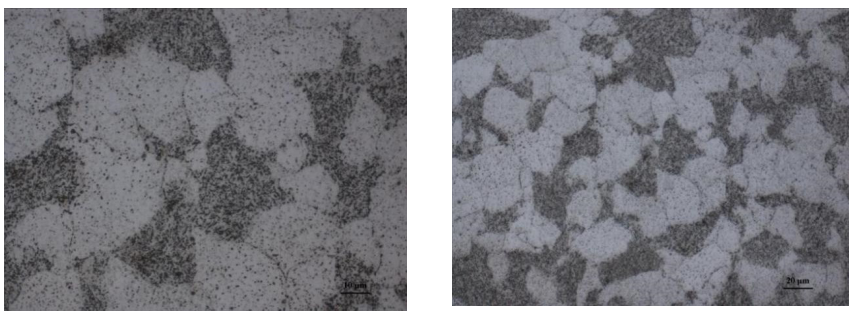

(**a**) (**b**)

**Figure 7.** Metallographic structure of inner surface in the 0°direction. (**a**) 500×, (**b**) 1000×.

### *2.4. Life Assessment*

#### 2.4.1. Creep Test

According to GB/T 2039-2012 (uniaxial tensile creep test method for metallic materials) [23], constant load creep tests at five stress levels were carried out at 540 °C and 580 °C. The creep test results showed that the longest fracture time was 6948 h at 540 °C and 148 MPa, and the endurance test lasted 11,012 h at 540 °C and 125 MPa. After the creep test, fracture of the sample was achieved and its micro morphology was observed under a scanning electron microscope, as shown in Figures 8 and 9. We observed that the macro-fracture morphology was cup-shaped, and the micro-fracture morphology covered the fiber area and shear lip area, and no radiation area was observed. Significant plastic deformation occurred throughout the entire creep process.

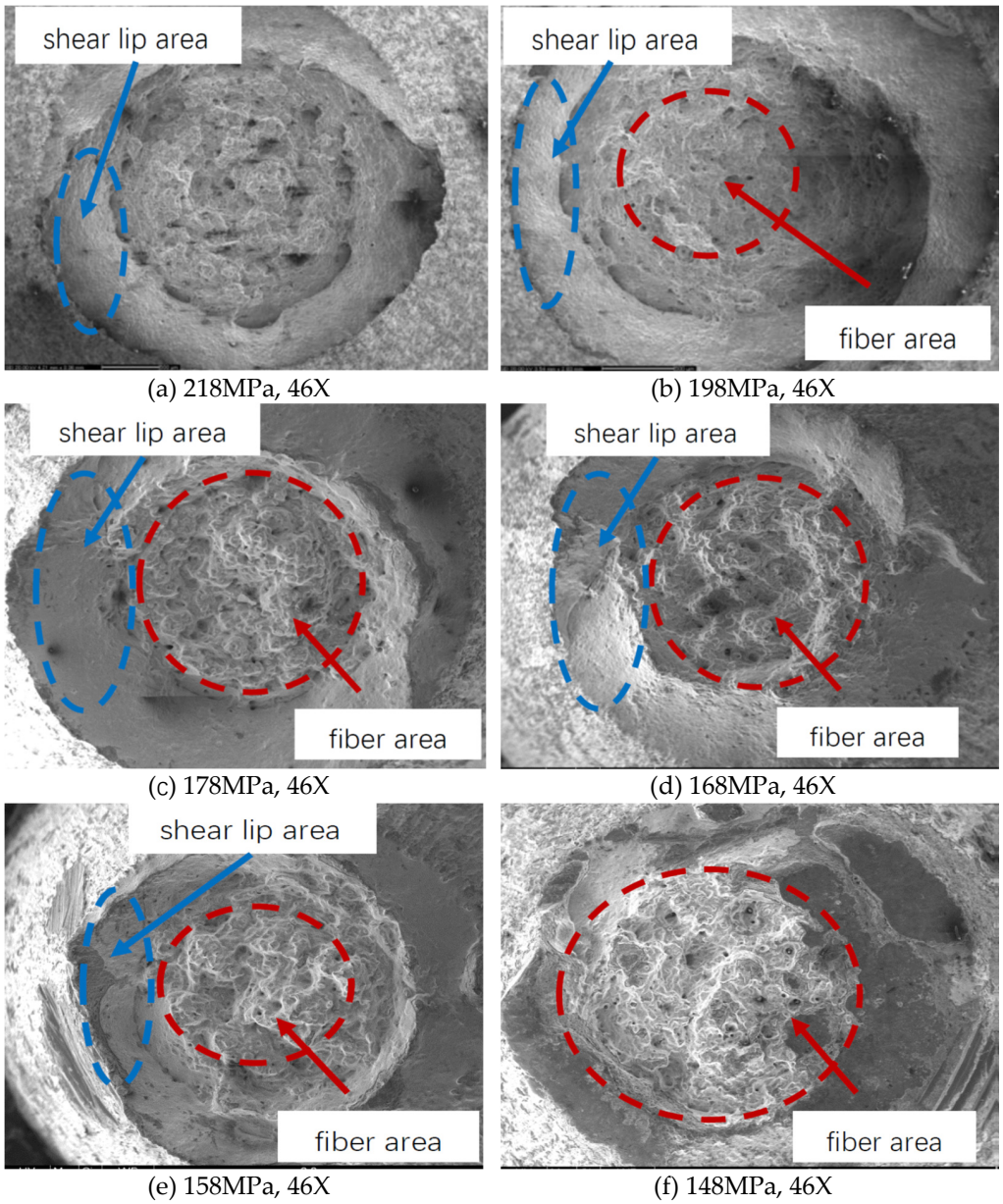


**Figure 8.** Fracture morphology of the 540 °C creep specimen.

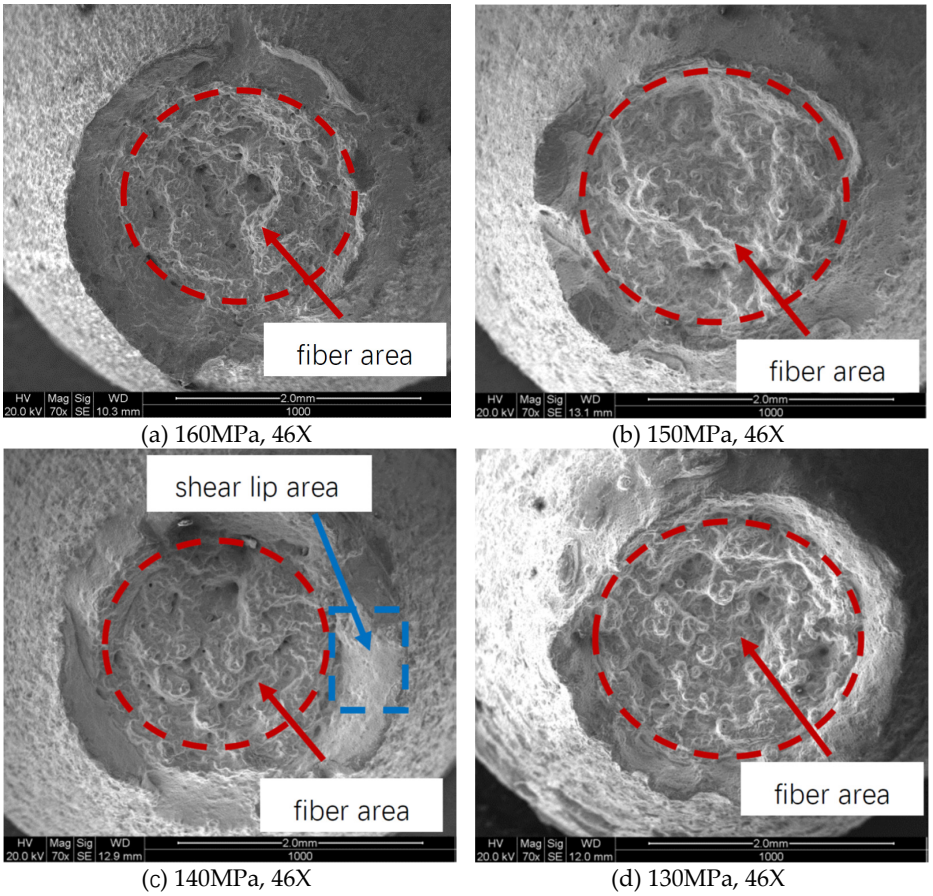


(a) 160MPa, 46X (b) 150MPa, 46X

(c) 140MPa, 46X (d) 130MPa, 46X

**Figure 9.** Fracture morphology of the 580 °C creep specimen.

2.4.2. Calculation of the Working Stress

CAESAR II software was used to analyze the stress of the P22 steel pipe. According to the data provided by the service manufacturer, a pipe system model was established. Following the relevant basic parameters of the P22 pipe, the maximum stress was calculated to be 112 MPa (Figure 10, A point). From the high-temperature tensile test and data, Rp0.2 = 268 MPa, Rm = 427 MPa, and E = 173,500,000 Pa were achieved at 540 °C, and E = 210,980,000 Pa, coupled with a Poisson's ratio of 0.3, was achieved at room temperature.

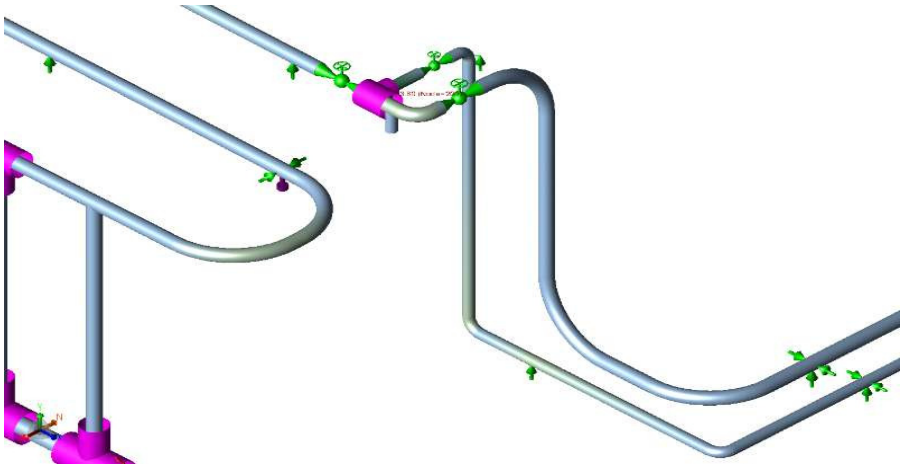

**Figure 10.** The location diagram of the maximum stress point.

2.4.3. Assessment of Residual Life

Compared to the traditional extrapolation prediction method, the $\theta$ parameter prediction method more fully considered the entire creep process and more accurately reflected the deformation characteristics of the materials, so that the residual creep life of the P22 steel pipe was predicted by the $\theta$ parameter prediction method in this paper.

2.4.3.1. Basic Principles of the $\theta$ Parameter Method

(1) A group of samples was tested at different temperatures and stress levels, and the creep fracture curves of each sample at a certain temperature and stress were obtained.
(2) We used Equation (1) to fit the creep fracture curve of each sample under different temperatures and stresses, and solved $\theta_i$ ($i$ = 1, 2, 3) in the creep equation of each sample:

$$\varepsilon = \theta_1 t + \theta_2 \left( e^{\theta_3 t} - 1 \right) \quad (1)$$

where and are the rate parameters of the second and third stages of creep, is the deformation parameter of the third stage of creep, and $t$ is the time of creep.

(1) We used $\theta_i$ from Equation (1), the temperature of the test ($T$), and the stress ($\sigma$) to obtain $a_i$, $b_i$, $c_i$, and $d_i$ in Equation (2). On this foundation, the relationship between $\theta_i$, $T$, and $\sigma$ was established.

$$lg^{\theta_i} = a_i + b_i\sigma + c_i T + d_i \sigma T \quad (2)$$

where coefficients $a_i$, $b_i$, $c_i$, and $d_i$ are independent with stress and temperature.

(2) We used $a_i$, $b_i$, $c_i$, and $d_i$ achieved in Equation (2) to allocate $\theta_i$ under the condition of specified temperature and pressure. Then, $\theta_i$ was substituted into Equation (1) to obtain the material creep curve.
(3) As stipulated in DL/T 940-2005 (technical guidelines for life assessment of steam pipes in thermal power plants) [24], the creep life can be determined by determining the creep strain at the transition tangent point from the second stage (approximate straight line) to the third stage as the failure point on the creep deformation curve of materials under the service conditions of steam pipes.

2.4.3.2. Extrapolation Analysis

According to the creep fracture curves of the creep tests at 540 °C and 580 °C, the $\theta_i$ values were obtained by the quasi-Newton method (BFGS) and general global optimization method, as shown in Table 7.

**Table 7.** The values of $\theta_i$ at different stress levels at 540 °C and 580 °C.

| Temperature (°C) | Stress (MPa) | $\theta_1$ | $\theta_2$ | $\theta_3$ |
|---|---|---|---|---|
| 540 | 218 | $1.3458 \times 10^{-3}$ | $9.9846 \times 10^{-6}$ | 0.0733 |
| | 208 | $3.1977 \times 10^{-4}$ | $2.3522 \times 10^{-6}$ | 0.02743 |
| | 198 | $2.3577 \times 10^{-4}$ | $1.3341 \times 10^{-6}$ | 0.0201 |
| | 178 | $3.4904 \times 10^{-5}$ | $9.5889 \times 10^{-6}$ | 0.0035 |
| | 168 | $4.7631 \times 10^{-5}$ | $2.5901 \times 10^{-6}$ | 0.0041 |
| 580 | 170 | $7.6631 \times 10^{-4}$ | $3.4986 \times 10^{-6}$ | 0.0596 |
| | 160 | $2.8969 \times 10^{-4}$ | $2.0798 \times 10^{-6}$ | 0.0294 |
| | 150 | $1.6092 \times 10^{-4}$ | $4.2577 \times 10^{-7}$ | 0.0186 |
| | 140 | $1.0447 \times 10^{-4}$ | $2.1470 \times 10^{-6}$ | 0.0103 |

When the temperature was constant, it had a linear relationship between $\lg\theta_i$ with $\sigma_i$. Using the relevant data in Table 7, the values of $a_i$, $b_i$, $c_i$, $d_i$ were obtained by linear fitting, as shown in Table 8.

**Table 8.** The fitting coefficient of $\theta_i$.

| $\theta_i$ | a | b | c | d |
|---|---|---|---|---|
| $\theta_1$ | −74.6496 | 0.2222 | 0.07810 | −0.0002 |
| $\theta_2$ | 55.1724 | −0.3212 | −0.0739 | 0.0004 |
| $\theta_3$ | −61.4492 | 0.1739 | 0.0656 | −0.0002 |

After T = 813 k and σ = 112 MPa were input into Equation (2), the results were incorporated into Equation (1) to obtain Equation (3):

$$\varepsilon = (1.1480E-7)t + (6.8346E-6)(e^{(2.9546E-5)t} - 1) \quad (3)$$

Using Equation (2), the creep fracture curve of P22 pine under the working conditions of 540 °C and 9.58 MPa was drawn, as shown in Figure 11. According to DL/T940-2005 "Technical guidelines for the life assessment of steam pipelines in thermal power plants", the residual creep life was determined to be 226,205 h, and the specific location is shown in Figure 11. The P22 steel pipe could operate for another 29 years if operated for 7800 h per year.

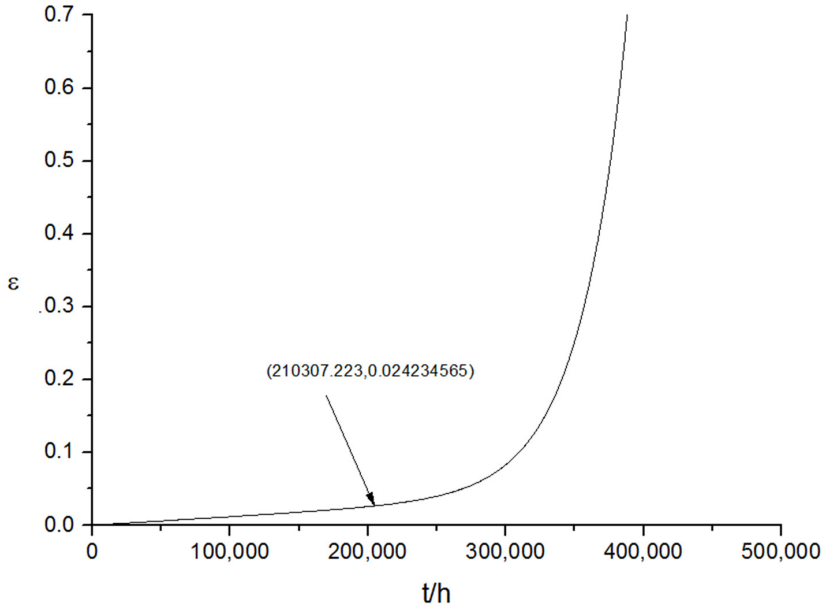


**Figure 11.** The creep fracture curve of the P22 pine.

## 3. Conclusions

In this study, a series of comprehensive physical and chemical tests were carried out for a replaced P22 steam pipeline, and the comprehensive properties of the P22 pipeline materials under the current state were analyzed. On this basis, high-temperature tensile and creep tests were carried out. Based on the $\theta$ parameter extrapolation method and the creep test results, the creep residual life of the P22 steam pipeline was scientifically predicted. The results showed that the P22 steam pipeline could still operate for more than 200,000 h and nearly 30 years.

Considering the evaluation results, several suggestions were put forward.

(a) During actual operation, the operating parameters of the P22 steam pipeline should be strictly monitored to allow it to operate under allowable operating conditions, to avoid safety events.

(b) In the next periodic inspection and shutdown maintenance, the P22 steam pipeline should be the main inspection object to receive attention. If necessary, the service cycle of the P22 steam pipeline could be shortened.

**Author Contributions:** Methodology, Z.W. and Y.Y.; analysis, Y.Y., Z.W. and B.W.; writing—original draft preparation, B.W. and L.D.; writing—review and editing, Z.W.; visualization, Z.W. and L.D.; funding acquisition, Z.W. All authors have read and agreed to the published version of the manuscript.

**Funding:** This research was funded by the energy saving technology integration and application demonstration project of typical high energy consuming industrial equipment (NO.2018YFF0216) and the research on integrity management technology of petrochemical equipment based on big data (KJ204103).

**Institutional Review Board Statement:** Not applicable.

**Informed Consent Statement:** Not applicable.

**Data Availability Statement:** Data available on request from the authors.

**Acknowledgments:** This work was financially supported by the energy saving technology integration and application demonstration project of typical high energy consuming industrial equipment (NO.2018YFF0216) and the research on integrity management technology of petrochemical equipment based on big data (KJ204103). Mailing mailbox: wangzc@gmx.com.

**Conflicts of Interest:** The authors declare no conflict of interest.

## References

1. Zhao, X.; Ma, X.; Chen, B.; Shang, Y.; Song, M. Challenges toward carbon neutrality in China: Strategies and countermeasures. Resources. *Conserv. Recycl.* **2022**, *176*, 105959. [CrossRef]
2. Tozer, L.; Klenk, N. Discourses of carbon neutrality and imaginaries of urban futures. *Energy Res. Soc. Sci.* **2018**, *35*, 174–181. [CrossRef]
3. Subramanian, C. Dissimilar metal weld failure of steam piping in a hydrogen unit of petroleum refinery. *Eng. Fail. Anal.* **2021**, *134*, 105983. [CrossRef]
4. Kim, D.J.; Kim, S.W.; Lee, J.Y.; Kim, K.M.; Oh, S.B.; Lee, G.G.; Kim, J.; Hwang, S.-S.; Choi, M.J.; Lim, Y.S.; et al. Flow-accelerated corrosion assessment for SA106 and SA335 pipes with elbows and welds. *Nucl. Eng. Technol.* **2021**, *53*, 3003–3011. [CrossRef]
5. Hayakawa, H.; Nakashima, S.; Kusumoto, J.; Kanaya, A.; Nakashima, H. Creep deformation characterization of heat resistant steel by stress change test. *Int. J. Press. Vessel. Pip.* **2009**, *86*, 556–562. [CrossRef]
6. Frank, A.; Pinter, G.; Lang, R.W. Prediction of the remaining lifetime of polyethylene pipes after up to 30 years in use. *Polym. Test.* **2009**, *28*, 737–745. [CrossRef]
7. Frank, A.; Arbeiter, F.J.; Berger, I.J.; Hutař, P.; Náhlík, L.; Pinter, G. Fracture mechanics lifetime prediction of polyethylene pipes. *J. Pipeline Syst. Eng. Pract.* **2019**, *10*, 04018030. [CrossRef]
8. Maleki, S.; Zhang, Y.; Nikbin, K. Prediction of creep crack growth properties of P91 parent and welded steel using remaining failure strain criteria. *Eng. Fract. Mech.* **2010**, *77*, 3035–3042. [CrossRef]
9. Holmström, S.; Pohja, R.; Nurmela, A.; Moilanen, P.; Auerkari, P. Creep and creep-fatigue behaviour of 316 stainless steel. *Procedia Eng.* **2013**, *55*, 160–164. [CrossRef]
10. Viswanathan, R. Life management of high-temperature piping and tubing in fossil power plants. *J. Press. Vessel Technol.* **2000**, *122*, 305–316. [CrossRef]
11. Kumar, M.; Singh, I.V.; Mishra, B.K.; Ahmad, S.; Rao, A.V.; Kumar, V. A modified theta projection model for creep behavior of metals and alloys. *J. Mater. Eng. Perform.* **2016**, *25*, 3985–3992. [CrossRef]
12. Holmström, S. Engineering Tools for Robust Creep Modelling. Ph.D. Thesis, VTT, Espoo, Finland, 2010.
13. Hamata, N.L.M.; Shibli, I.A. Creep crack growth of seam-welded P22 and P91 pipes with artificial defects. Part II. Data analysis. *Int. J. Press. Vessel. Pip.* **2001**, *78*, 827–835. [CrossRef]
14. Demofonti, G.; Mannucci, G.; Hillenbrand, H.G.; Harris, D. Evaluation of the suitability of X100 steel pipes for high pressure gas transportation pipelines by full scale tests. In Proceedings of the International Pipeline Conference, Calgary, AL, Canada, 4–8 October 2004; Volume 41766, pp. 1685–1692.
15. Rathod, D.W.; Pandey, S.; Singh, P.K.; Prasad, R. Mechanical properties variations and comparative analysis of dissimilar metal pipe welds in pressure vessel system of nuclear plants. *J. Press. Vessel. Technol.* **2016**, *138*, 011403. [CrossRef]
16. Vilkys, T.; Rudzinskas, V.; Prentkovskis, O.; Tretjakovas, J.; Višniakov, N.; Maruschak, P. Evaluation of failure pressure for gas pipelines with combined defects. *Metals* **2018**, *8*, 346. [CrossRef]
17. Liu, S.; Yang, C.; Peng, Z. An approach to 570 °C/105 h creep rupture strength prediction and safety assessment of Grade 91 components with reduced hardness after service exposures at 530–610 °C. *Int. J. Press. Vessel. Pip.* **2020**, *182*, 104073. [CrossRef]
18. Yin, Z.; Cai, H.; Liu, H.G. Performance of heat-resistant steel P 92 used in 1000 MW ultra supercritical unit after long-term service at high temperature. *Trans. Mater. Heat Treat.* **2012**, *33*, 105–110.
19. *GB/T 228.1-2010*; Metallic Materials-Tensile Testing-Part 1: Method of Test at Room Temperature. Standardization Administration of the People's Republic of China (SAC): Beijing, China, 2010.

20. Mehari, Z.A.; Han, J. Effects of the partial heating roll forming method on springback of high strength steel. *Int. J. Adv. Manuf. Technol.* **2022**, *119*, 5195–5210. [CrossRef]
21. Yang, C.; Li, X.; Wang, Y.; Sun, M. Failure Analysis and Protection of Oxygen Corrosion of Reheater Tube in a Power plant. In *E3S Web of Conferences*; EDP Sciences: Les Ulis, France, 2021; p. 261.
22. Yu, H.; Peng, X.; Lian, Z.; Zhang, Q.; Shi, T.; Wang, J.; Zhao, Z. Experimental and numerical simulation of fatigue corrosion behavior of V150 high-strength drill pipe in air and H2S-dilling mud environment. *J. Nat. Gas Sci. Eng.* **2022**, *98*, 104392. [CrossRef]
23. Zhang, B.; Zhang, S.; Du, H.; Yao, Z.; Kong, X.S.; Tao, X. Dependence of Creep Properties on Aging Treatment in Al-Cu-Mg Alloy. *Adv. Eng. Mater.* **2022**, *24*, 2101293. [CrossRef]
24. Zhu, B.; Xia, X.; Xiao, J.; Tang, M.; Ma, Q.; Shi, J.; Xue, F.; Zhang, G. Research on the residual life of the superheating system steam header for an extended service 220 MW ultra-high voltage thermal power unit. *Int. J. Press. Vessel. Pip.* **2021**, *194*, 104513. [CrossRef]